Muon-catalyzed *dd* fusion between 25 and 150 K: Theoretical analysis

A. Scrinzi, P. Kammel, J. Zmeskal, W. H. Breunlich, and J. Marton
Institut für Mittelenergiephysik, Österreichische Akademie der Wissenschaften, Boltzmanngasse 3, A-1090, Vienna, Austria

M. P. Faifman and L. I. Ponomarev
Kurchatov Atomic Energy Institute, Moscow 123182, Russia

T. A. Strizh
Joint Institute for Nuclear Research, Dubna 141980, Russia

(Received 26 May 1992; revised manuscript received 22 February 1993)

We present a detailed theoretical analysis of experimental rates for $dd\mu$ molecular formation and $d\mu$ hyperfine transitions at temperatures 25.5–150 K, which were reported by Zmeskal *et al.* [Phys. Rev. A **42**, 1165 (1990)]. Theoretical effective $dd\mu$ formation rates are fitted to the observed rates by adjusting the $dd\mu$ binding energy ε_{11}, the effective *dd* fusion rate $\bar{\lambda}_f$, and the nonresonant $dd\mu$ formation rate λ_{nr}. The value of $\varepsilon_{11}=-1966.1\pm0.2$ meV is determined with extreme accuracy and agrees with the theoretical prediction within 0.1 meV. Experimental findings for λ_{nr} are compatible with theory. Since the value of $\bar{\lambda}_f$ extracted from observed formation rates depends on the calculated value of $dd\mu$ formation matrix elements $|V_{if}|$, we present the region of pairs $(\bar{\lambda}_f,|V_{if}|)$ allowed by experiment. The theoretical values of $\bar{\lambda}_f$ and $|V_{if}|$ lie outside this region. A significant discrepancy remains for the $d\mu$ hyperfine transitions, where the theoretical rates, which consist of scattering and back-decay contributions, exceed experimental rates by ~40%. Fits of the experimental data indicate that mostly the scattering contribution is smaller than calculated. The extrapolation of our fit to higher temperatures is in good agreement with other experiments on $dd\mu$ formation.

PACS number(s): 36.10.Dr, 34.50.−s

I. INTRODUCTION

In extensive experimental and theoretical studies the catalysis of nuclear fusion reactions by muons in hydrogen isotope mixtures has been investigated, covering a wide variety of phenomena ranging from atomic and nuclear to weak-interaction physics (see recent reviews in Refs. [1,2]). Among the various investigations a substantial contribution came from the analysis of muon-catalyzed fusion (μCF) in pure deuterium, which has been distinguished by a particularly fruitful interaction between theory and experiment.

In the 1960s the observation of an unexpectedly strong temperature dependence of the neutron flux from *dd* fusions after injection of muons into deuterium [3] led to the discovery of a new resonant process for the formation of the muonic molecule $dd\mu$, which eventually revived interest in the whole field of μCF. The mechanism, which was proposed by Vesman [4], allowed one to explain the high intensity and the temperature dependence of the neutron flux by resonant formation of the $dd\mu$ molecule, provided it had an extremely weakly bound state.

Over the following ten years an effective scheme for the calculation of such a loosely bound excited state of $dd\mu$ and similar systems was developed, which used the adiabatic representation of the three-body Coulomb problem [5] and allowed one to calculate the binding energies within an accuracy of ~10–100 meV [6–8]. Based on these results a first tentative calculation of the temperature dependence of resonant $dd\mu$ formation was undertaken [9]. The calculation was found to be in qualitative agreement with a first experiment [10], which measured the $dd\mu$ formation rate in a wider temperature range.

The observation of a dramatic dependence of the $dd\mu$ formation rate on the hyperfine states of $d\mu$ [11] stimulated further efforts to achieve detailed quantitative understanding of μCF in pure deuterium: the relativistic and hyperfine structures of $d\mu$ and $dd\mu$ [12,13] as well as the rovibrational excitations of the D_2 molecule and of the $[(dd\mu)dee]$ mesic molecular complex [14–16] were taken into account; the contributions to $dd\mu$ formation of all partial waves of the $d\mu+D_2$ relative motion [14] and the electron screening of the interaction between $d\mu$ and D_2 [17] were included; it was realized that the nonequilibration of the ortho-para distribution of D_2 cannot be neglected [18]. Once rates of $dd\mu$ deexcitation [19] and of nuclear fusion [20] had been calculated, it was recognized that the process of back decay of $[(dd\mu)dee]$ [21–24] competes strongly with fusion. A separate program was devoted to accurately calculate cross sections of $d\mu$ scattering on deuterium [25]. Inelastic scattering cross sections with hyperfine transitions were obtained in qualitative agreement with experiment [11]. When finally high-precision variational calculations [26–30] pushed the accuracy of the purely Coulombic $dd\mu$ energies to about 0.1 meV and the relativistic corrections [31–34] could be refined correspondingly, the first completely *ab initio* calculation on the basis of Ref. [35] of all

relevant rates of μCF in pure deuterium could be presented [36].

In the meantime experiments had been performed in a wide range of temperatures in liquid and gaseous D_2 [37–43]. In particular the results of experiments [11,39–41], which studied the hyperfine effects in $dd\mu$ formation and the hyperfine transition rates, were used for the detailed comparison with the *ab initio* theory.

In a preceding paper [41] the results of an experiment [referred to in the following as the Vienna-PSI experiment (PSI indicates the Paul Scherrer Institute)] on the $dd\mu$ molecular formation and $d\mu$ hyperfine transition rates at temperatures between 25.5 and 150 K were reported. In this work we present the detailed theoretical analysis of these rates, whose main conclusions were already quoted in Ref. [41]. Relying on the calculation scheme of molecular formation [35,36,44], we have extracted the main characteristic parameters of muon catalysis in pure deuterium from fits to the mentioned experimental results. We have obtained the nonresonant formation rate λ_{nr}, the $dd\mu$ binding energy ε_{11} of the loosely bound state with rotational and vibrational quantum numbers $J=v=1$, and the correlation between the $[(dd\mu)dee]$ molecular formation matrix elements and the effective dd-fusion rate $\tilde{\lambda}_f$. We discuss the impact of theoretical inputs on the fit results and we compare experimental and theoretical findings for these parameters. Further we discuss the present theoretical understanding of the observed rate of hyperfine transitions in $d\mu$ atoms. Finally, we have extrapolated the fits to compare with $dd\mu$ formation rates in the whole range of temperatures up to 600 K observed in experiments [37,38,42,43].

II. THEORY

A. $dd\mu$ formation

The $dd\mu$ molecules are formed by the resonant mechanism in the excited state of angular momentum $J=1$ and vibrational quantum number $v=1$ with an energy of only $\varepsilon_{11}\approx -2$ eV, which is on the scale of ordinary molecular energies rather than on the muonic scale. (For comparison, the $dd\mu$ ground-state energy is $\varepsilon_{00}\approx -300$ eV.) Therefore the energy released in the formation of $dd\mu$ in this loosely bound state can be absorbed by excitations of rovibrational states of the hybrid mesic molecular complex $[(dd\mu)dee]$:

$$(d\mu)_F+(D_2)_{K_i\nu_i}\rightarrow[(dd\mu)_S dee]_{K_f\nu_f}\quad [=:(\mathrm{MD})_{K_f\nu_f}]\ . \tag{1}$$

Here $F=\frac{1}{2}$ and $\frac{3}{2}$ denote the mesic atom $d\mu$ hyperfine doublet ($\uparrow\downarrow$) and quartet ($\uparrow\uparrow$) states, respectively, and $(K_i\nu_i)$ are the rovibrational quantum numbers of D_2. The quantum numbers of the $dd\mu$ hyperfine state are $S=\frac{1}{2}$ and $\frac{3}{2}$ and by $(K_f\nu_f)$ we denote the rovibrational quantum numbers of the hybrid complex MD, in which the $M^+\equiv(dd\mu)^+$ ion acts as a heavy hydrogen nucleus. The spin-orbit (fine structure) splitting of the $dd\mu$ levels, which is two orders of magnitude smaller than the hyperfine splitting [34], was found to be negligible for our analysis and has been omitted here.

By equating initial and final energies in reaction (1), one obtains the resonance condition for the relative $d\mu$-D_2 kinetic energy ε_{if},

$$\varepsilon_{if}=\varepsilon_{11}+\delta\varepsilon_{dd\mu}(S)+E_{\mathrm{MD}}(K_f,\nu_f)-\varepsilon_{d\mu}-\delta\varepsilon_{d\mu}(F)-E_{\mathrm{D}_2}(K_i,\nu_i)\ , \tag{2}$$

where E_{MD} and E_{D_2} denote the energies of the MD and D_2 rovibrational states relative to the D+D dissociation energy, respectively. Following convention the $d\mu$ and $dd\mu$ energies $\varepsilon_{d\mu}$ and ε_{11} are given relative to the $d\mu+d$ threshold implying $\varepsilon_{d\mu}\equiv 0$. The energy ε_{11} of an isolated $dd\mu$ molecule consists of the binding energy of the Coulomb three-body system with corrections for relativistic effects, vacuum polarization, and nuclear structure [34]. In the definition of ε_{11} we include an additional correction for the interaction of $dd\mu$ with the surrounding electrons due to the finite size of the $dd\mu$ ion [45–47]. The hyperfine energy shifts of $d\mu$ and $dd\mu$ [34] are denoted by $\delta\varepsilon_{d\mu}$ and $\delta\epsilon_{dd\mu}$, respectively.

For negligible widths of the resonance and assuming thermalization of $d\mu$ atoms the rate of process (1) at temperature T and density N of D atoms is given by the formula [36,44]

$$\lambda_{FK_i,SK_f}(T)=2\pi N f(\varepsilon_{if},T)\omega_i(K_i)W_{FS}|V_{if}|^2\ . \tag{3}$$

Here $f(\varepsilon_{if},T)=2(\varepsilon_{if}/\pi)^{1/2}(k_BT)^{-3/2}\exp(-\varepsilon_{if}/k_BT)$ is the Maxwell distribution of the $d\mu$–D_2 kinetic energies and $|V_{if}|$ is the transition matrix element from the initial (F,K_i) state to the final (S,K_f) state. Vibrational quantum numbers were omitted, since at temperatures $\lesssim 1000$ K only $\nu_i=0$ and $\nu_f=7$ contribute [36]. The overlap between the initial and final spin functions after averaging over magnetic quantum numbers and symmetrizing under permutation of all three deuterons is

$$W_{FS}=2(2S+1)\begin{Bmatrix}\frac{1}{2} & 1 & F\\ 1 & S & 1\end{Bmatrix} \tag{4}$$

(the curly brackets denote the Wigner $6j$ symbol). The occupation probability $\omega_i(K_i)$ of D_2 rotational states has the following functional form:

$$\omega_i(K_i)\propto[(2K_i+1)\xi(K_i)\exp(-E_{\mathrm{D}_2}(K_i)/k_BT)]\ , \tag{5}$$

where

$$\xi(K_i)=\begin{cases}\frac{1}{3}\ , & \text{for } K_i=\text{odd}\ ,\\ \frac{2}{3}\ , & \text{for } K_i=\text{even}\end{cases} \tag{6}$$

accounts for the spin multiplicity of even and odd (ortho and para) states of D_2. In thermal equilibrium the K_i states are Boltzmann distributed with the normalization $\sum_{K_i}\omega_i(K_i)=1$. However, since transitions with a change in the symmetry of the D_2 spin function are strongly suppressed [48], total symmetry under dd exchange suppresses transitions between even and odd rotational states. The target filling procedure of the Vienna-PSI experiment produced ortho and para D_2 in statistical proportions, i.e., at a ratio 2:1, and this ratio was conserved

throughout the experiment. Therefore the $\omega_i(K_i)$ have to be normalized separately for even and odd states so that

$$\sum_{K_i=\text{even}} \omega_i(K_i)=\tfrac{2}{3} , \quad \sum_{K_i=\text{odd}} \omega_i(K_i)=\tfrac{1}{3} . \tag{7}$$

Here we would like to mention the possibility of collisional broadening of the resonances, which has been discussed in Refs. [49–52]. For a rough estimate of the possible resonance width in the Vienna-PSI experiment we scale the rather large value of ≈ 10 meV [50] for the width in liquid D_2 to gas density. Since the 25.5-K data were obtained at only 2% of liquid-hydrogen density, the width reduces to about 0.2 meV. This value of the linewidth in gas is indeed negligible compared to the width of ≈ 2 meV of the Maxwell distribution at the given target temperature. Moreover, note that the assumptions of Ref. [50] leading to the large width have been criticized in Ref. [52].

The nonresonant molecular formation rate λ_{nr} describes the process of $dd\mu$ formation where the released energy is carried off by a conversion electron. It is composed of a term independent of energy (and temperature) and one increasing linearly with temperature, corresponding to $dd\mu$ formation from $d\mu+d$ scattering in an s wave and a p wave, respectively [53,54]:

$$\lambda_{\text{nr}}=\lambda_1+\lambda_2\tfrac{3}{2}k_B T . \tag{8}$$

B. *dd* fusion and back decay

Nuclear dd fusion in $[(dd\mu)dee]$ may either occur directly from the excited $dd\mu$ $(J=1,v=1)$ state, or it may be preceded by stabilization of $[(dd\mu)dee]$ through deexcitation of $dd\mu$. Since the dipole $E1$ transition of $dd\mu$ $(J=1,v=1)$ to $J=0$ states requires a change of the symmetry of the spin function, such dipole transitions are forbidden in the nonrelativistic limit. The monopole $E0$ transition to the $(J=1, v=0)$ state is quite slow $\lambda_{\text{dex}}=22$ μs^{-1} [19]. For this reason fusion mainly occurs from the $dd\mu$ $(J=1,v=1)$ state with the rate $\lambda_f^{\text{th}}=440$ μs^{-1} [20], which is comparatively slow due to the centrifugal barrier between the nuclei. Thus, the effective rate leading to fusion after $[(dd\mu)dee]$ formation is equal to

$$\tilde{\lambda}_f^{\text{th}}=\lambda_f^{\text{th}}+\lambda_{\text{dex}}\approx 460\ \mu\text{s}^{-1} . \tag{9}$$

Instead of undergoing fusion, the excited $[(dd\mu)dee]$ complex can also decay back to $d\mu+D_2$. The back-decay rate is strictly connected with the formation rate equation (3) by the formula [36]

$$\Gamma_{SK_f,F'K_i'}=\frac{(2m^3\varepsilon_{if})^{1/2}}{\pi}\xi(K_i')\frac{2F'+1}{2S+1}\frac{2K_i'+1}{2K_f+1}W_{F'S}|V_{if}|^2 \tag{10}$$

with the $d\mu+D_2$ reduced mass $m^{-1}=m_{d\mu}^{-1}+(2m_d)^{-1}$.

Equation (10) is appropriate for dense targets, where collisions with neighboring target molecules lead to the mixing of states with different magnetic quantum numbers of the angular momenta K_f and J. It was pointed out [55] that at very low densities this mixing will be incomplete and formation, collisional relaxation, and decay of the eigenstates of total angular momentum $\mathcal{J}=\mathbf{K}_f+\mathbf{J}$ should be considered. In the present paper, however, target densities of 2–5% of liquid hydrogen are analyzed where we expect that the magnetic substates are at least partially mixed in collisions, so that the averaged expressions used provide a reasonable approximation (see also Sec. III B and Appendix A).

Back decay has a significant influence on the $dd\mu$ reaction kinetics [23,24,36,41] since according to calculations [36], the back-decay rates Γ_{SK_f,FK_i} exceed the effective fusion rate $\tilde{\lambda}_f$ by a factor of ≈ 3, i.e., only one out of four $[(dd\mu)dee]$ complexes proceeds to fusion. Since in experiments only the fusion reactions are detected, one observes the effective formation rates [36]

$$\tilde{\lambda}_F=\lambda_{\text{nr}}+\sum_{K_iSK_f}\lambda_{FK_i,SK_f}w_S^{\text{fus}}(K_f) , \tag{11}$$

where the resonant rates λ_{FK_i,SK_f} are reduced by the fusion fractions w_S^{fus}.

The fusion fractions w_S^{fus} depend in a nontrivial way on the degree to which the $(\text{MD})_{K_f}$ states are thermalized before back decay or fusion. The correct way to calculate w_S^{fus} in the general case is given in Appendix A. Only two extreme cases can be written down straightforwardly.

(a) If there are no transitions between different K_f states, the fusion fraction w_S^{fus} is given by

$$w_S^{\text{fus}}(K_f)\approx\frac{\tilde{\lambda}_f}{\tilde{\lambda}_f+\sum_{F'K_i'}\Gamma_{SK_f,F'K_i'}} . \tag{12}$$

As discussed above this formula provides only an approximate expression for the fusion fractions at very low target densities since it assumes complete mixing of the magnetic substates of K_f.

(b) If the rates of K_f transitions are much higher than the back-decay rates Γ_{SK_f,FK_i} and the fusion rate $\tilde{\lambda}_f$, the rotational states will generally be thermalized before back decay or fusion. In this case the back-decay rates are averaged over the Boltzmann distribution [denoted by $\omega_f(K_f)$] and the fusion fraction is

$$w_S^{\text{fus}}(K_f)\approx\frac{\tilde{\lambda}_f}{\tilde{\lambda}_f+\sum_{F'}\Gamma_{SF'}} , \quad \Gamma_{SF'}=\sum_{K_iK_f}\omega_f(K_f)\Gamma_{SK_f,F'K_i} . \tag{13}$$

In *liquid* targets, where the rates of transitions $(\text{MD})_{v_fK_f}\rightarrow(\text{MD})_{v_fK_f'}$ due to collisions with the surrounding D_2 molecules [56] exceed back decay and fusion rates by at least two orders of magnitude, Eq. (13) is applicable. At the conditions of the Vienna-PSI experiment—densities of 2% and 5% of liquid hydrogen and low temperatures—the rotational relaxation rates are of the same order as the back-decay rates. Therefore only partial thermalization of the MD rotational states is achieved before back decay and one has to use w_S^{fus} given in Appendix A.

In this context it has to be mentioned that *vibrational* deexcitation of MD may contribute to the effective fusion rate, since after the loss of a vibrational quantum (≈ 300 meV) the back-decay channel is closed. Following Ref. [57] one can estimate the rate of vibrational transitions of MD using the transition rate of D_2 as the upper limit by relying on experimental evidence [58] that the rates decrease with growing masses. The value obtained this way of $\lesssim 20\ \mu s^{-1}$ for liquid D_2 is one order of magnitude smaller than the effective fusion rate. For low-density gas the effect is negligible.

C. Hyperfine transitions

The second important process in the kinetics, hyperfine transitions, can either proceed through inelastic $d\mu + D_2$ scattering

$$d\mu(F) + D_2 \rightarrow d\mu(F') + D_2 , \quad F \neq F' , \tag{14}$$

or through intermediate formation of $[(dd\mu)dee]$

$$d\mu(F) + D_2 \rightarrow [(dd\mu)_S dee] \rightarrow d\mu(F') + D_2 . \tag{15}$$

Accordingly, the effective hyperfine transition rates $\tilde{\lambda}_{FF'}$ are composed of a scattering and a back-decay part [24,36]

$$\tilde{\lambda}_{FF'} = \lambda_{FF'}^{\text{scat}} + \lambda_{FF'}^{\text{back}} , \tag{16}$$

where the back-decay contribution is given by

$$\lambda_{FF'}^{\text{back}} = \sum_{K_i SK_f} \lambda_{FK_i,SK_f} w_{SF'}^{\text{back}}(K_f) . \tag{17}$$

In analogy to the fusion fraction w_S^{fus} in Eq. (11), $w_{SF'}^{\text{back}}(K_f)$ is defined as the fraction of back decay from $[(dd\mu)_S dee]_{K_f}$ to the $d\mu(F')$ hyperfine state. Again for the extreme case of very low and very high target densities approximate formulas such as (12) and (13) can be readily written down (the general case is discussed in Appendix A).

From experimental neutron time spectra only three independent rates can be extracted while four effective rates enter the kinetics [Eq. (10) in Ref. [41]]. Two of these rates, the upward and downward hyperfine transition rates, are connected by the detailed-balance relation

$$\begin{aligned} \tilde{\lambda}_{1/2,3/2}(T) &= 2e^{\Delta\varepsilon_{\text{hf}}/k_B T} \tilde{\lambda}_{3/2,1/2}(T) \\ &= 2e^{-564/T\,(\text{K})} \tilde{\lambda}_{3/2,1/2}(T) \end{aligned} \tag{18}$$

with $\Delta\varepsilon_{\text{hf}} \equiv \delta\varepsilon_{d\mu}(F=\frac{1}{2}) - \delta\varepsilon_{d\mu}(F=\frac{3}{2})$. This relation holds rigorously only if D_2 and MD rotational states are in thermal equilibrium (see Appendix B), but, as calculations show, deviations from this relation due to the nonequilibration of ortho and para D_2 and rotational $(\text{MD})_{K_f}$ states are well below the level of 1% at temperatures $\gtrsim 90$ K and are also negligible at lower temperatures because of the exponential suppression of the upward hyperfine rate $\tilde{\lambda}_{1/2,3/2}$.

III. FIT OF THE $dd\mu$ FORMATION RATES

The Vienna-PSI experiment observed the effective molecular formation rates $\tilde{\lambda}_{1/2}$, $\tilde{\lambda}_{3/2}$, and the hyperfine transition rate $\tilde{\lambda}_{3/2,1/2}$ at temperatures between 25.5 and 150 K and at densities of 2% and 5% of liquid hydrogen. We have compiled these rates in Table I together with results from other relevant experiments performed by the Vienna-PSI group. As usual the trivial linear density dependency has been removed by scaling the observed rates to liquid-H_2 density $N_0 = 4.25 \times 10^{22}$ atoms/cm^3.

A. Fit model

According to the theory discussed above, the following more fundamental quantities determine the formation rates $\tilde{\lambda}_F$ in Eq. (11): the nonresonant formation rate λ_{nr}, the effective fusion rate $\tilde{\lambda}_f$, the resonance energies ε_{if}, the $dd\mu$ formation matrix elements $|V_{if}|$, and the MD rotational transition rates.

In the fits the constant λ_1 and linear λ_2 term of the nonresonant rate λ_{nr} [Eq. (8)] and the effective fusion rate $\tilde{\lambda}_f$ were directly used as fit parameters. The MD rotational transition rates, which at the densities considered enter the fusion and back-decay fractions w_S^{fus} and $w_{SF'}^{\text{back}}$ in a nontrivial way, turned out to have relatively little impact on the results (see below) and were therefore taken from calculation [56]. Of the energies entering the resonance energies ε_{if} [Eq. (2)] the rovibrational spectra E_{MD} and E_{D_2} and the hyperfine energies $\delta\varepsilon_{d\mu}$ and $\delta\varepsilon_{dd\mu}$ are known with sufficient accuracy (the values used are given in Tables II and III). The remaining $dd\mu$ binding energy ε_{11} served as the fourth fit parameter.

The matrix elements $|V_{if}|$ crucially enter the initial formation rates λ_{FK_i,SK_f} [Eq. (3)] as well as the back-decay rates $\Gamma_{SK_f,F'K_i'}$ [Eq. (10)]. However, it is difficult to estimate the accuracy of the approximations used to calculate the matrix elements $|V_{if}|$ [44]. In a recent attempt [59] to go beyond the dipole approximation, which had

TABLE I. Rates $\tilde{\lambda}_{1/2}$, $\tilde{\lambda}_{3/2}$, and $\tilde{\lambda}_{3/2,1/2}$ from experiments at PSI. The rates are normalized to liquid-hydrogen density and given in μs^{-1}. (For the results of Ref. [41] only relative errors are given. The error from the absolute calibration of the whole data set results in an additional error of 8.4% for $\tilde{\lambda}_F$ and 1% for $\tilde{\lambda}_{3/2,1/2}$, respectively.)

Ref.	T (K)	$\tilde{\lambda}_{1/2}$	$\tilde{\lambda}_{3/2}$	$\tilde{\lambda}_{3/2,1/2}$
[41]	25.5	0.0468(54)	3.46(13)	36.0(1.0)
	40.0	0.0469(25)	3.76(18)	36.8(0.9)
	70.0	0.0769(45)	3.67(20)	34.8(1.1)
	95.0	0.191(23)	4.14(20)	32.7(1.7)
	117.0	0.455(36)	4.54(29)	35.8(2.7)
	150.0	0.864(61)	4.99(25)	37.3(2.8)
[11]	34.8	0.045(5)	3.8(4)	37.0(1.5)
[39]	45.0	0.045(3)	3.74(25)	36.6(1.5)
[40]	23.8	0.050(4)	3.25(33)	30.50(0.72)

TABLE II. Rotational quanta of D_2 ($v_i=0$, K_i) and [$(dd\mu)dee$] ($v_f=7$, K_f) in meV. E_0 are the ground-state energies relative to the D+D dissociation threshold. The values are accurate to at least 0.05 meV [16].

K	D_2 ($v=0$) $E_0=-4556.215$	[$(dd\mu)dee$] ($v=7$) $E_0=-4584.382$
0	0.0	2026.007
1	7.412	2030.393
2	22.202	2039.150
3	44.303	2052.244
4	73.614	2069.628
5	110.005	2091.236
6	153.315	2116.992
7	203.358	2146.803
8	259.924	2180.566
9	322.782	2218.163

been used as the standard approximation for the interaction operator until then, the value of $|V_{if}|$ obtained for the $dt\mu$ system is by a factor of $\approx\sqrt{2}$ smaller than in Ref. [44]. In similar calculations for $dd\mu$, which due to *dd* permutation symmetry are not completely justified, however, we obtained qualitatively similar results. Compared to the previous calculation [44] all matrix elements decreased by an overall constant factor. Therefore, in order to investigate the dependence of our fit results on the matrix elements we introduced a scaling factor α: $|V_{if}|^2\rightarrow\alpha|V_{if}|^2$, with $|V_{if}|$ from Ref. [44].

In this way the effective molecular formation rates

$$\tilde{\lambda}_F(T)=\lambda_1+\lambda_2\tfrac{3}{2}k_BT + \sum_{K_iSK_f}\alpha\lambda_{FK_i,SK_f}(T;\varepsilon_{11})w_S^{\rm fus}(K_f;\alpha,\tilde{\lambda}_f) \quad (19)$$

were parametrized by the four physical quantities λ_1, λ_2, $\tilde{\lambda}_f$, ε_{11}, and the scaling parameter α. In a series of fits to all the rates $\tilde{\lambda}_F$ measured in the Vienna-PSI experiment α was kept fixed at values between 0.2 and 2 (see explanation below), while λ_1, λ_2, $\tilde{\lambda}_f$, and ε_{11} were optimized according to maximum likelihood. The error in absolute calibration, which equally affects all $\tilde{\lambda}_{1/2}$ and $\tilde{\lambda}_{3/2}$ data points (cf. Ref. [41]), was taken into account by explicitly introducing the calibration into the χ^2 function as a fit parameter c which is constrained around $c=1\pm\sigma_c$,

$$\chi^2=\sum_{F,i}\left[\frac{c\tilde{\lambda}_F(T_i)-\tilde{\lambda}_F^{\rm expt}(T_i)}{\sigma_{F,i}}\right]^2+\left[\frac{1-c}{\sigma_c}\right]^2, \quad (20)$$

TABLE III. Hyperfine energy shifts $\delta\varepsilon_F$ and $\delta\varepsilon_S$ of $(d\mu)_F$ and $(dd\mu)_S$ in meV [34].

State	$\delta\varepsilon$
$d\mu$ ($F=\frac{1}{2}$)	−32.3
$d\mu$ ($F=\frac{3}{2}$)	16.2
$dd\mu$ ($S=\frac{1}{2}$)	−16.0
$dd\mu$ ($S=\frac{3}{2}$)	8.0

where the sum is taken over the experimental rates $\tilde{\lambda}_F^{\rm expt}(T_i)$ with errors $\sigma_{F,i}$ from Ref. [41] (cf. Table I). The absolute calibration error is $\sigma_c=0.084$ [41].

The scaling parameter α must be $\gtrsim 0.2$, since otherwise $\tilde{\lambda}_F<\tilde{\lambda}_F^{\rm expt}$ (note that always $w_S^{\rm fus}<1$). For all values $\alpha\geq 0.2$ the data can be fitted with χ^2 values between 4 and 7. At a total of eight degrees of freedom this means satisfactory compatibility of the fit function with data for all α. Figure 1 shows the fit obtained with the value $\alpha=1$.

The reason for the good compatibility of the fit function with the data in this wide range of α is a strong correlation between the effective fusion rate λ_f and α (see Fig. 2). This can be demonstrated by using $w_S^{\rm fus}$ from Eq. (13). We insert Eq. (13) into Eq. (11), neglect λ_{nr}, include α, and sum over K_i and K_f to obtain

$$\tilde{\lambda}_F\approx\sum_S\alpha\lambda_{FS}\frac{\tilde{\lambda}_f}{\tilde{\lambda}_f+\sum_{F'}\alpha\Gamma_{SF'}}, \qquad \lambda_{FS}\equiv\sum_{K_i,K_f}\lambda_{FK_i,SK_f}. \quad (21)$$

Obviously, as long as $\tilde{\lambda}_f$ and $\alpha\Gamma_{SF'}$ are comparable in size, an increase of $\alpha\lambda_{FS}$, i.e., initial $dd\mu$ formation, can be compensated for by a reduction of $\tilde{\lambda}_f$, leading to a smaller fusion fraction. For values $\alpha>2$ the fits become independent of α since then $\tilde{\lambda}_f\ll\alpha\Gamma_{SF}$ and the α dependence of Eq. (21) cancels.

This behavior is clearly reflected in Fig. 2: For all values above $\alpha\gtrsim 0.2$ one finds a corresponding $\tilde{\lambda}_f$ to fit the observed λ_F. While initially $\tilde{\lambda}_f$ quickly decreases with increasing α, the dependency levels out when α approaches 2.

B. $dd\mu$ binding energy

Most remarkably, the fit parameter ε_{11} is only weakly correlated with all other parameters. In particular, the variation of α from 0.2 to 2 changes ε_{11} by no more than 0.16 meV. Thus, choosing $\alpha=1$, we were able to extract the accurate $dd\mu$ binding energy

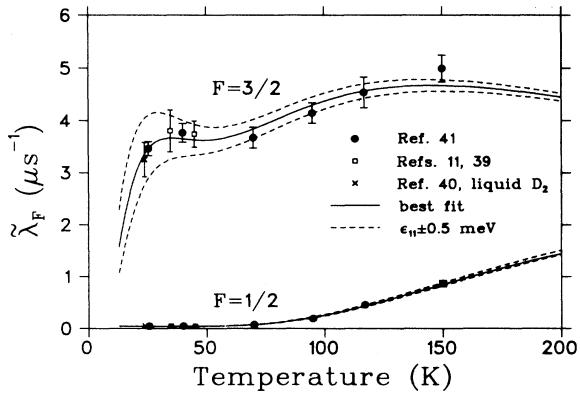

FIG. 1. Molecular formation rates $\tilde{\lambda}_{1/2}$ and $\tilde{\lambda}_{3/2}$ from all experiments performed at PSI and fits from this work. The dashed lines show the sensitivity of the rates to shift of ε_{11} by ± 0.5 meV.

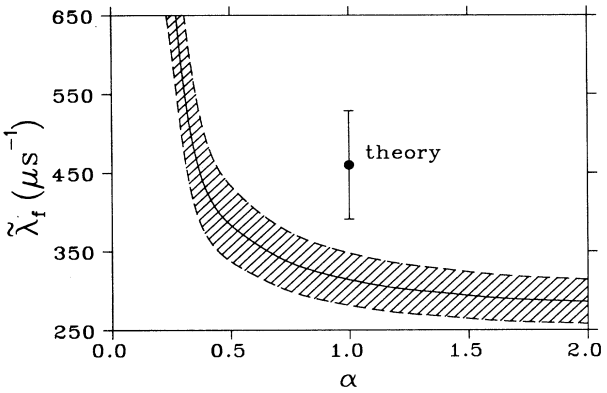

FIG. 2. The allowed region ($\pm 1\sigma$ errors) of $(\tilde{\lambda}_f, \alpha)$ as extracted from experimental $\tilde{\lambda}_F$. Note the correlation between α and $\tilde{\lambda}_f$. The uncertainty of $\tilde{\lambda}_f^{\text{theory}}$ is estimated to be 15% [64].

$$\varepsilon_{11} = -1966.1 \pm 0.2 \text{ meV} . \quad (22)$$

The error equals the quadratic sum of the 1σ statistical error of 0.16 meV, 0.1 meV for the variation with α (Table VI), and 0.05 meV for uncertainties in the rovibrational spectra of D_2 and MD [15,16]. Compared to Ref. [41] the error could be reduced by omitting the estimated error contribution from the hyperfine structure of $dd\mu$ since by now the theoretical values are well established [34].

Note that it is the measurement of the temperature dependence of the $\tilde{\lambda}_{3/2}$ rate in the Vienna-PSI experiment that allows this extremely accurate determination of ε_{11}. This is due to the fact that $\tilde{\lambda}_{3/2}$ at temperatures $\lesssim 50$ K is dominated by the low-lying resonances $(F=\frac{3}{2}, K_i=0) \rightarrow (S=\frac{1}{2}, K_f=1)$, $(F=\frac{3}{2}, K_i=1) \rightarrow (S=\frac{1}{2}, K_f=2)$, and $(F=\frac{3}{2}, K_i=2) \rightarrow (S=\frac{3}{2}, K_f=1)$, which are located at 4.0, 5.3, and 5.8 meV, respectively (Table IV), and whose contributions vary sharply with ε_{11} (cf. Fig. 3). If in Eq. (3) we neglect the influence of $\omega_i(K_i)$, we see that for a given resonance the maximum of λ_{FK_i,SK_f} (assumed at $\varepsilon_{if} = k_B T$) is $\propto 1/\varepsilon_{if}$. Therefore a small shift (≈ 0.5 meV) of the resonances to lower (higher) energies strongly enhances (suppresses) the low-temperature bump in the $\tilde{\lambda}_{3/2}$ rate, while the same shift hardly affects the rates at higher temperatures (see inset in Fig. 3). This sensitivity of the $\tilde{\lambda}_{3/2}$ *temperature dependence* to ε_{11} decouples ε_{11} from $\tilde{\lambda}_f$ and α, which predominantly act on the *absolute value* of resonant $dd\mu$ formation. The theoretical $\tilde{\lambda}_{3/2}$ is compatible with the data only in a very small range of ε_{11}: the dashed lines in Fig. 1 result from a shift of ε_{11} by ± 0.5 meV from the optimum value. The $\tilde{\lambda}_{1/2}$ rate and the steady-state rate $\tilde{\lambda}_{dd\mu}$ (see Sec. V) are far less sensitive to the exact value of ε_{11}, since they have no resonances at low energies.

The experimental fact of the nonthermalized, statistical ortho-para distribution of D_2 enters the rates since the D_2 total nuclear spin states of the low-lying resonances are different: the $K_i=0$ and $K_i=2$ states are ortho, and $K_i=1$ is a para state of D_2. The resonances are separated

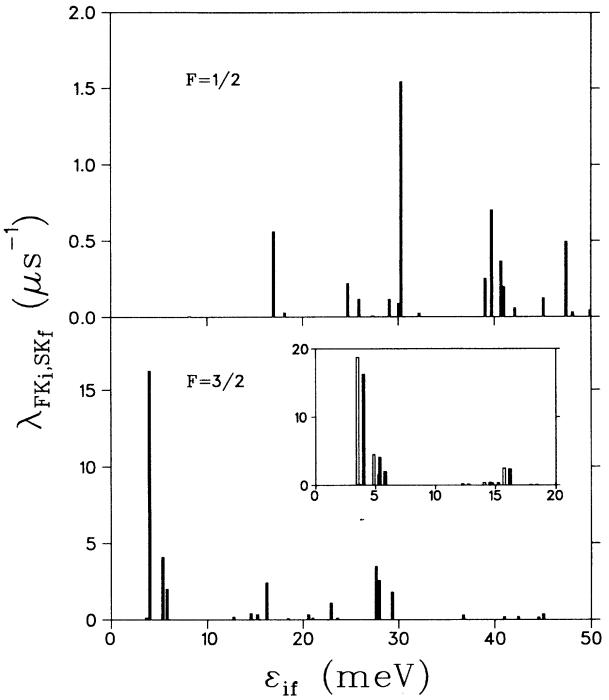

FIG. 3. Strengths of the resonances of $dd\mu$ formation. For each resonance the formation rate $\lambda_{K_i F, K_f S}$ was evaluated at $T = \varepsilon_{if}/k_B$. The empty bars in the inset show the sensitivity of the lowest resonances to a shift of the resonance energies by 0.5 meV.

by 1.3 meV which corresponds to ≈ 10 K. Now, comparing to D_2 in thermal equilibrium, a bigger fraction of D_2 will be in the $K_i=1$ state, thus shifting the initial bump in the $\tilde{\lambda}_{3/2}$ rate to higher temperatures and suppressing it. In a fit, this emphasis of the higher ($K_i=1$) resonance is compensated by a shift of all ε_{if} to lower energies. From Eq. (2) one sees that this means a decrease in ε_{11}. Since this decrease amounts to 0.6 meV, it is essential to use the ortho-para distribution which correctly describes the experimental conditions (in our case this is the statistical distribution).

The small, but significant effect of nonthermalization of the MD rotational states was studied by using Eq. (A8) from Appendix A, which is an approximate expression to account for the competition between back decay and collision-induced relaxation of the states with rotational quantum numbers K_f. We fitted the experimental rates $\tilde{\lambda}_F$ with three different expressions for the fusion fraction: w^{fus} from Eq. (13) corresponding to complete relaxation of K_f states, w^{fus} from Eq. (12) corresponding to no transitions between K_f states, and w^{fus} from Eq. (A8) for partial relaxation of K_f calculated for the experimental densities ($\Phi = 2$–5 % of liquid-H_2 density). The effect of no relaxation shifts ε_{11} by -0.6 meV relative to complete relaxation. For the calculated relaxation relative to complete relaxation a shift of only -0.2 meV was found and included in the final result. We note that in the derivation of Eqs. (12) and (A8) statistical mixing of the mag-

netic substates of K_f and J was assumed, while at extremely low densities the total angular momentum $\mathcal{J}=\mathbf{K}_f+\mathbf{J}$ of the intermediate molecular complex remains conserved [55]. At the densities considered in the present paper, partial mixing of the magnetic substates of K_f will occur in collisions, which, however, is difficult to estimate, since no detailed transition rates are available [60]. We observe, however, that the values of ε_{11} are very similar for the fits with the calculated relaxation and with complete relaxation. This suggests that significant rotational transitions occur prior to back decay, which will also partially mix the magnetic quantum numbers. Accordingly, the averaged expressions used in Eq. (A8) should provide a reasonable approximation for the experimental target densities considered.

Finally we would like to discuss the significance of using only a single constant scaling factor α for all matrix elements $|V_{if}|^2$. It can be understood from the preceding discussion that a change in the ratio between $\tilde{\lambda}_{3/2}$ at high and low temperatures will directly influence ε_{11}. Although at present there are no indications that the $|V_{if}|^2$ for $dd\mu$ scale differently for different resonances, we would like to quantify the sensitivity of ε_{11} to an energy dependence of the scaling factor α.

It turns out that the key quantity is the ratio of α at the upper group of resonances at ~ 30 meV (see Table IV and Fig. 3) over α at the threshold resonances at ~ 4 meV. Figure 4 shows the deviation $\Delta\varepsilon_{11}$ from ε_{11} (obtained with $\alpha\equiv 1$) as a function of the ratio $\alpha(30\text{ meV})/\alpha(4\text{ meV})$. Several different functional forms of the energy dependence of α were tested. One sees that quite independently of the functional shape of $\alpha(\varepsilon_{if})$ there is an approximate linear relation

$$\Delta\varepsilon_{11}\approx(2.5\text{ meV})\times[\alpha(30\text{ meV})/\alpha(4\text{ meV})-1]\ . \tag{23}$$

It is interesting to note that for all functional shapes of $\alpha(\varepsilon_{if})$ used the fits favor a constant α and seem to rule out an energy dependence of $|\alpha(30\text{ meV})/\alpha(4\text{ meV})-1|\gtrsim 0.3$. In any case, if future calculations should lead to significant energy-dependent modifications of the formation matrix elements $|V_{if}|^2$, the simple relation equation (23) will allow one to correct ε_{11} correspondingly.

C. Nonresonant formation parameters

The fit results for the nonresonant formation parameters λ_1 and λ_2 almost exclusively depend on the low-temperature data for $\tilde{\lambda}_{1/2}$. Because of the 48.5-meV $d\mu$ hyperfine splitting, all resonances with the $F=\frac{1}{2}$ initial state are located at high energies (see Table IV and Fig. 3) leaving us with purely nonresonant formation for $\tilde{\lambda}_{1/2}$ at temperatures $\lesssim 50$ K. These points are, of course, not affected by the values of ε_{11}, $\tilde{\lambda}_f$, and α. Since the p-wave contribution must rise with the energy, we subject it to the constraint $\lambda_2\geq 0$. The fit values are

$$\lambda_1=0.044\pm 0.005\ \mu\text{s}^{-1} \tag{24}$$

and

$$\lambda_2\lesssim 1.0\ \text{eV}^{-1}\text{s}^{-1}\ . \tag{25}$$

TABLE IV. Energies and matrix elements of the most important resonance transitions in $[(dd\mu)dee]$ formation. Atomic units (a.u.) are defined by $m_e=\hbar=e=1$.

			$F=\frac{3}{2}$		$F=\frac{1}{2}$	
S	K_i	K_f	ε_{if} (meV)	$\lvert V_{if}\rvert^2$ (10^{-10} a.u.)	ε_{if} (meV)	$\lvert V_{if}\rvert^2$ (10^{-10} a.u.)
$\frac{1}{2}$	3	2			16.96	0.166
$\frac{3}{2}$	4	3			24.74	0.151
$\frac{1}{2}$	2	1			30.30	0.152
$\frac{1}{2}$	2	2			39.06	0.035
$\frac{1}{2}$	4	5			39.73	0.201
$\frac{1}{2}$	1	0			40.71	0.124
$\frac{3}{2}$	3	2			40.96	0.142
$\frac{1}{2}$	3	4			47.44	0.205
$\frac{1}{2}$	2	3			52.15	0.215
$\frac{1}{2}$	0	1	4.00	0.483	52.50	0.360
$\frac{1}{2}$	1	2	5.35	0.320	53.85	0.240
$\frac{3}{2}$	2	1	5.80	0.173	54.30	0.130
$\frac{3}{2}$	4	5			63.73	0.170
$\frac{3}{2}$	1	0	16.20	0.141		
$\frac{1}{2}$	2	4			69.54	0.067
$\frac{3}{2}$	2	3	27.65	0.246	76.15	0.183
$\frac{3}{2}$	0	1	28.00	0.413		
$\frac{3}{2}$	1	2	29.35	0.274		

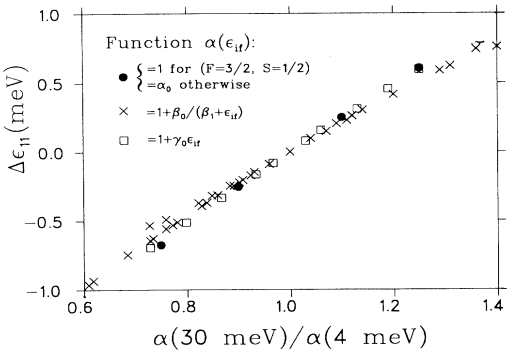

FIG. 4. Influence of energy dependence of α on ε_{11}. $\Delta\varepsilon_{11}$ is the shift relative to ε_{11} obtained with $\alpha\equiv 1$. The parameter β_1 was varied between 5 and 40 meV. The shift almost exclusively depends on the ratio $\alpha(30\text{ meV})/\alpha(4\text{ meV})$ and is virtually independent of the functional form of $\alpha(\varepsilon_{if})$.

The errors are somewhat larger than those given in Ref. [41] since the correlation between λ_1 and λ_2 has been included in the present analysis.

IV. HYPERFINE TRANSITION RATES

For the analysis of the hyperfine transition rates $\tilde{\lambda}_{3/2,1/2}$, we parametrized the back-decay contribution $\lambda^{\text{back}}_{3/2,1/2}$ in the same way as the molecular formation rate [cf. Eq. (19)],

$$\lambda^{\text{back}}_{3/2,1/2}(T)=\sum_{K_i SK_f}\alpha\lambda_{3/2,K_i,SK_f}(T,\varepsilon_{11})w^{\text{back}}_{S,1/2}(K_f;\alpha,\tilde{\lambda}_f)\ . \tag{26}$$

The detailed expression used for $w^{\text{back}}_{SF'}$ is given in Eq. (A9) of Appendix A. To demonstrate the dependence of $\lambda^{\text{back}}_{3/2,1/2}$ on α and $\tilde{\lambda}_f$ we use the same approximation as for Eq. (21),

$$\lambda^{\text{back}}_{3/2,1/2}\approx\sum_S\alpha\lambda_{3/2,S}\frac{\alpha\Gamma_{S,1/2}}{\tilde{\lambda}_f+\alpha\sum_{F'}\Gamma_{SF'}}\ . \tag{27}$$

Compared to Eq. (21) there is an additional α in the numerator leading to high sensitivity of $\lambda^{\text{back}}_{3/2,1/2}$ to α. In Fig. 5 $\lambda^{\text{back}}_{3/2,1/2}$ is calculated for $\alpha=0.36$, 0.5, and 1 with the remaining parameters chosen to fit the observed formation rates $\tilde{\lambda}^{\text{expt}}_F$: one sees that $\lambda^{\text{back}}_{3/2,1/2}$ is roughly proportional to α. Thus the back-decay contribution to the hyperfine transition rate provides a handle to determine the values of $\tilde{\lambda}_f$ and α. Unfortunately, there is no agreement between the theoretically predicted $\tilde{\lambda}_{3/2,1/2}$ and experimental data (Fig. 6). The calculated rate $\lambda^{\text{scat}}_{3/2,1/2}$ for the process $d\mu(\uparrow\uparrow)+D_2\rightarrow d\mu(\uparrow\downarrow)+D_2$ [61] is already bigger than the observed $\tilde{\lambda}_{3/2,1/2}$ rates. After adding $\lambda^{\text{back}}_{3/2,1/2}$ with the theoretical value $\alpha=1$ the total theoretical rates exceed the observed rates by $\approx 40\%$.

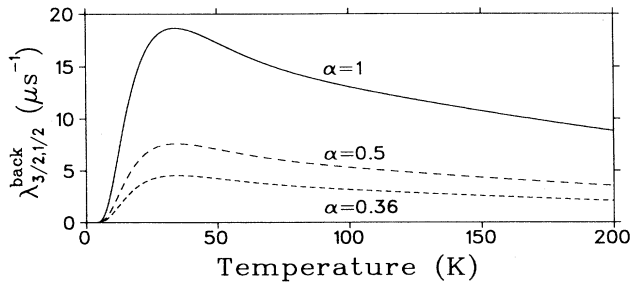

FIG. 5. Dependence on α of the back-decay contribution to the hyperfine transition rates. For each value of α the corresponding $\tilde{\lambda}_f$ was chosen according to Fig. 2.

The two contributions $\lambda^{\text{scat}}_{3/2,1/2}$ and $\lambda^{\text{back}}_{3/2,1/2}$ have quite a different temperature dependence: while $\lambda^{\text{scat}}_{3/2,1/2}$ is roughly linear, $\lambda^{\text{back}}_{3/2,1/2}$ reflects the resonant shape of $[(dd\mu)dee]$ formation. One can try to exploit this difference to separate the two contributions in the experimental rates. For that purpose we introduced an additional parameter β to scale $\lambda^{\text{scat}}_{3/2,1/2}\rightarrow\beta\lambda^{\text{scat}}_{3/2,1/2}$. This simple scaling is based on the assumption that the energy dependence of $d\mu+d$ scattering up to ≈ 50 meV≈ 400 K is determined only by phase space, a behavior found for the hyperfine transitions of all hydrogen isotopes at energies below 50 meV [25]. We further assume that the $\approx 10\%$ corrections due to electron screening and D_2 rotational excitations [61,62] scale proportionally to the $d\mu+d$ rate for bare nuclei. Then we have

$$\tilde{\lambda}_{3/2,1/2}=\lambda^{\text{back}}_{3/2,1/2}(\varepsilon_{11},\tilde{\lambda}_f,\alpha)+\beta\lambda^{\text{scat}}_{3/2,1/2}\ . \tag{28}$$

In simultaneous fits in $\tilde{\lambda}_{1/2}$, $\tilde{\lambda}_{3/2}$ by Eq. (19) and $\tilde{\lambda}_{3/2,1/2}$ by Eq. (28) all four parameters $\tilde{\lambda}_f$, ε_{11}, α, and β were determined. Here ε_{11} and the correlation between $\tilde{\lambda}_f$ and α predominantly depend on the molecular formation rates, while α and β are fixed by temperature dependence and absolute value of $\tilde{\lambda}_{3/2,1/2}$. Table VII and Fig. 7 present the fit results, which we obtained with two different shapes for $\lambda^{\text{scat}}_{3/2,1/2}$.

Fit (a) uses the most recent calculation of $\lambda^{\text{scat}}_{3/2,1/2}$ presented in Ref. [61], which includes D_2 molecular effects and electron screening.

Fit (b) with the bare nuclei $d\mu+d$ scattering rate [25] was included to show the effect of minor modifications of

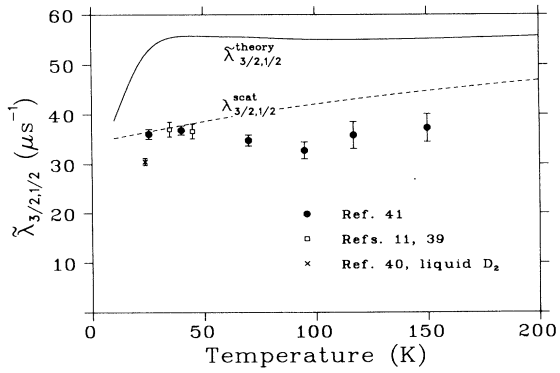

FIG. 6. Theoretical and experimental hyperfine transition rates. The theoretical $\lambda^{\text{scat}}_{3/2,1/2}$ already exceeds the measured rates. The total theoretical rates, which contain the back-decay contribution for $\alpha=1$, exceed the measured ones by $\approx 40\%$.

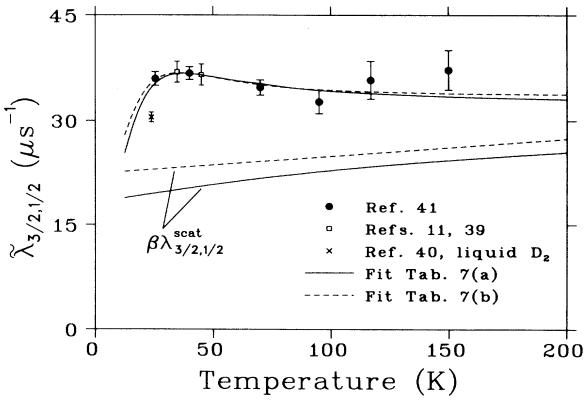

FIG. 7. Fits to the hyperfine transition rates according to Table VII. The two lower curves are the respective scattering contributions.

the shape of $\lambda^{scat}_{3/2,1/2}$ on the separation, and also because final agreement among theorists about electron screening has not been reached (Refs. [61,62]).

The errors in the fits are quite large. Yet (a) and (b) agree in showing a reduction of $\lambda^{scat}_{3/2,1/2}$ by $\approx 60\%$, where the scaled scattering rates $\beta\lambda^{scat}_{3/2,1/2}$ of both fits coincide within the statistical errors. Findings for $\lambda^{back}_{3/2,1/2}$ are compatible with no scaling of $|V_{if}|^2$ ($\alpha=1$), but a significant reduction of $|V_{if}|^2$ by up to $\alpha=0.6$ lies within the errors as well.

V. DISCUSSION

A. Comparison with theory

In the course of the efforts to obtain a complete theoretical description of muon-catalyzed fusion in pure deuterium, all fundamental parameters describing this process have been calculated. We are now able to test these results against the experimental values extracted in the preceding chapters.

Table V summarizes our results and the corresponding theoretical values. The parameters of nonresonant formation are compatible with theory. The constant term λ_1 lies 3σ above the most recent theoretical value [54], while the experimental error of λ_2 is too big to allow a significant comparison with theory.

Within the experimental error we find excellent agreement between the most recent theoretical value for ε_{11} and our result. Note that we added 0.24 meV to the theoretical value [34] to account for the $dd\mu$ molecule finite-size correction. (This value was estimated in Ref. [1] by comparison with the $dt\mu$ molecule finite-size correction [47] and earlier calculations [46].) One has to keep in mind that uncertainties in the deuteron polarizability limit the accuracy of the theoretical binding energy to ≈ 0.5 meV [34]. The fit value ε_{11} depends very little on specific assumptions (cf. Table VI). In particular, the exact values of the molecular formation matrix elements $|V_{if}|^2$, which serve as theoretical input in the fits, have little influence. The small variation of ε_{11} which results from scaling the transition matrix elements $|V_{if}|^2$ by a constant factor α has been included into the systematic error. The value of ε_{11} is more sensitive to energy-dependent scaling of $|V_{if}|^2$, where a variation of $\pm 10\%$ in the ratio $\alpha(30\text{ meV})/\alpha(4\text{ meV})$ would cause shifts of ± 0.25 meV. However, neither theory nor experiment support such energy-dependent scaling of $|V_{if}|^2$. Further one sees that for fits on this level of accuracy it was necessary to use the correct ortho-para D_2 distribution and to calculate w_S^{fus} and $w_{SF'}^{back}$ including the effect of incomplete rotational relaxation of MD.

The accuracy of the experimental $dd\mu$ energy value is even high enough to test hypothetical long-range nuclear forces between the deuterons. Bounds on the strength of such van der Waals like forces, which might cause either an inverse power law or a Yukawa potential were derived in Ref. [63] assuming agreement between theory and experiment of only 100 meV. We recalculated these bounds using the much more accurate agreement of $\lesssim 0.5$ meV. Although replacing the very crude estimate of the first-order energy shift used in Ref. [63] with the exact first-order shift weakened the bounds to a certain extent, the total improvement is still approximately two orders of magnitude for an inverse power-law force and one order of magnitude for the Yukawa-type potentials. Yet, even with this significant improvement the bounds remain poorer than those obtained by other methods [63].

The fourth physical parameter in our fits, the effective fusion rate $\tilde{\lambda}_f$, cannot be unambigously extracted from the experimental data since it directly depends on the value adopted for the scaling parameter α. Thus, at present we only determine the region of pairs $(\tilde{\lambda}_f,\alpha)$ compatible with experimental data within 1σ errors (Fig. 2). Note that this result depends on the absolute size of the observed formation rates $\tilde{\lambda}_F^{expt}$, which is subject to the systematic uncertainties connected with the absolute calibra-

TABLE V. Results of the fit to $\tilde{\lambda}_{1/2}$ and $\tilde{\lambda}_{3/2}$ and theoretical values.

Quantity	Fit	Calculation	Ref.
ε_{11} (meV)	$-1966.1(2)$	-1966.2^a	[34]
λ_1 (μs^{-1})	0.044(5)	0.03	[54]
λ_2 ($eV^{-1}\mu s^{-1}$)	$\lesssim 1.0$	1.8	[54]
$\tilde{\lambda}_f$ ($\alpha=1.0$)	314(33)		
$\tilde{\lambda}_f$ ($\alpha=0.5$) (μs^{-1})	386(51)	460	[20,19]
$\tilde{\lambda}_f$ ($\alpha=0.36$)	461(87)		

[a]Includes an estimated $dd\mu$ finite-size correction of $+0.24$ meV [1].

TABLE VI. Influence of deviations from standard theory on ε_{11}.

Deviation from standard theory	Shift relative to $\varepsilon_{11}=-1966.1$ meV	χ^2
$\alpha\equiv 0.2$	+0.06	7
$\alpha\equiv 2.0$	−0.10	4
$\alpha(30\text{ meV})/\alpha(4\text{ meV})=1.0\pm 0.1$	±0.25	$\lesssim 5$
D_2 ortho-para equilibrium	+0.60	3.6
K_f thermal equilibrium	+0.20	4.6
no K_f transitions	−0.40	6.9

tion of neutron detectors [41].

As given, the theoretical point ($\tilde{\lambda}_f=460,\alpha=1$) lies well outside the experimentally allowed region of ($\tilde{\lambda}_f,\alpha$). Considering an uncertainty in the theoretical value of $\approx 15\%$ [64] the disagreement is not dramatic, nevertheless it suggests that either $\tilde{\lambda}_f$ or the matrix elements $|V_{if}|$ be smaller than calculated. It has been argued that indeed the dipole approximation for the interaction operator used in Ref. [44] overestimates $|V_{if}|^2$ [59]. The analogous squared matrix elements for the $dt\mu$ system were found to be overestimated in dipole approximation by a factor of 2 [59], i.e., $\alpha=0.5$. It is very likely that qualitatively the same holds for the $dd\mu$ matrix elements, but at present we cannot make a quantitative statement about the value of α for $dd\mu$. With the theoretical value for the fusion rate $\tilde{\lambda}_f^{\text{theory}}=460\ \mu\text{s}^{-1}$ we obtain $\alpha=0.36$ from the data (Fig. 2, Table V).

The discrepancy between theoretical and observed hyperfine transition rates is not yet understood. Here one has to emphasize that the experimental rates are subject to little systematic errors, since they mostly depend on the decay constant in neutron time spectra (cf. Ref. [41]), and that all experiments in D_2 gas [11,39,41] are consistent. Apparently the theoretical $\lambda_{3/2,1/2}^{\text{scat}}$ and possibly also $\lambda_{3/2,1/2}^{\text{back}}$ are too big. The separation of $\lambda_{3/2,1/2}^{\text{scat}}$ and $\lambda_{3/2,1/2}^{\text{back}}$ on grounds of their different temperature dependence indicates a reduction of $\lambda_{3/2,1/2}^{\text{scat}}$ by a factor $\beta\approx 0.6$. The corresponding back-decay contribution $\lambda_{3/2,1/2}^{\text{back}}$ within statistical and systematic errors is equally compatible with both the original unscaled matrix elements $|V_{if}|^2$ [44] or a significant reduction of the $|V_{if}|^2$, which has been predicted in Ref. [59].

B. Density effects

As mentioned in the theoretical introduction (Sec. II) there is the possibility of nonlinear density effects because at increased density (a) the width of the $dd\mu$ formation resonances might increase, (b) collisional relaxation of the excited [$(dd\mu)dee$] complex speeds up, and (c) vibrational relaxation of the complex might become significant. The experimental data discussed so far were obtained with gaseous D_2 targets of low density. These results can be compared with the experiment of Nägele *et al.* [40], where the $dd\mu$ formation rates and hyperfine transition rates were determined in a liquid-D_2 target (data points with the symbol × in Figs. 1, 6, and 7). For a quantitative analysis we have to extrapolate the gas data (lowest temperature 25.5 K) to the slightly lower temperature of the experiment with liquid D_2 (23.8 K). For definiteness we used the fit parameters of Table VII, fit (a), to calculate the extrapolated rates $\tilde{\lambda}_F^{\text{gas}}$ and $\tilde{\lambda}_{3/2,1/2}^{\text{gas}}$, where the errors of the extrapolated values result from the errors of the fit parameters. Now we can compare the rates from liquid and gas targets at equal temperature:

$$\begin{aligned}
&\tilde{\lambda}_{1/2}^{\text{gas}}=0.047(4)\ ,\quad \tilde{\lambda}_{1/2}^{\text{liq}}=0.050(4)\ ,\\
&\tilde{\lambda}_{3/2}^{\text{gas}}=3.36(34)\ ,\quad \tilde{\lambda}_{3/2}^{\text{liq}}=3.25(33)\ ,\\
&\tilde{\lambda}_{3/2,1/2}^{\text{gas}}=35(1)\ ,\quad \tilde{\lambda}_{3/2,1/2}^{\text{liq}}=30.5(9)\ .
\end{aligned}\tag{29}$$

As expected, the nonresonant formation rate $\tilde{\lambda}_{1/2}$ does not show a density dependence. Also the resonant $dd\mu$ formation rate $\tilde{\lambda}_{3/2}$ agrees between gas and liquid targets with the accuracy of the comparison limited by the quadratic sum of the errors to $\approx 15\%$. The hyperfine transition rate $\tilde{\lambda}_{3/2,1/2}$ on the other hand decreases significantly at liquid density. In the extrapolation used the back-decay contribution to $\tilde{\lambda}_{3/2,1/2}$ is $\lambda_{3/2,1/2}^{\text{back}}=15.4\ \mu\text{s}^{-1}$, which might be decreased by effect (a), i.e., collisional resonance broadening. For example, a resonance width of ≈ 10 meV would lead to decreases in the initial formation rates λ_{FK_i,SK_f} by the order of 25% [51], which would result in a similar decrease of $\lambda_{3/2,1/2}^{\text{back}}$ and $\tilde{\lambda}_{3/2}$. Although the rates $\tilde{\lambda}_{3/2}$ in Table (29) seem independent of density, such a decrease of the rate in liquid D_2 cannot be completely ruled out, given the large errors of the data. For $\tilde{\lambda}_{3/2,1/2}$ a $\sim 25\%$ decrease of the back-decay contribution might explain the observed drop of $4.5\ \mu\text{s}^{-1}$.

Density effects due to (b) and (c) are expected to remain within the experimental errors. Based on the theoretical cross sections of Ref. [56], we find that complete thermalization of the MD rotational states causes a rise of $\tilde{\lambda}_{3/2}$ by 7% in liquid D_2. Likewise the influence of vibrational deexcitation rates $\lesssim 20\ \mu\text{s}^{-1}$ on $\tilde{\lambda}_{3/2}$ remains below 5%. Both mechanisms affect $\lambda_{3/2,1/2}^{\text{back}}$ by no more than 2%.

TABLE VII. Results from simultaneous fits to $\tilde{\lambda}_{1/2}$, $\tilde{\lambda}_{3/2}$, and $\tilde{\lambda}_{3/2,1/2}$. Parametrization $\tilde{\lambda}_{3/2,1/2}=\lambda_{3/2,1/2}^{\text{back}}(\varepsilon_{11},\alpha,\tilde{\lambda}_f)+\beta\lambda_{3/2,1/2}^{\text{scat}}$. In both fits $\varepsilon_{11}=1966.1(2)$ meV.

Fit	$\lambda_{3/2,1/2}^{\text{scat}}$	β	α	$\tilde{\lambda}_f$
(a)	Ref. [61]	0.54(7)	0.91(15)	320(34) μs^{-1}
(b)	Ref. [25]	0.67(9)	0.76(16)	337(40) μs^{-1}

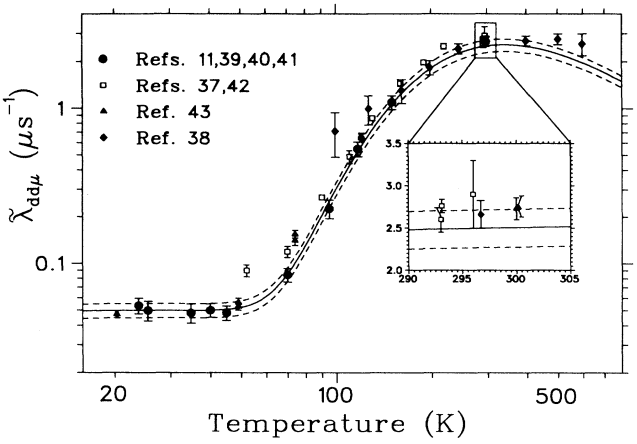

FIG. 8. Summary of theoretical and experimental results on steady-state molecular formation rates. The fit to the PSI data is extrapolated to higher temperatures (solid line). Dashed lines indicate the 1σ errors of the fit.

C. Comparison with other experiments

In Fig. 8 experimental $dd\mu$ formation rates for the whole range of temperatures investigated up to now are compiled [11,37–43]. Some older measurements have been omitted, in particular in cases where an accurate interpretation is difficult by now and where results have been updated by the most recent generation of experiments (cf. Ref. [41] for these older data). For the comparison of experiments one has to notice that only experiments [11,39–41] separate the basic rates $\tilde{\lambda}_{1/2}$ and $\tilde{\lambda}_{3/2}$. For other experiments these rates have been separated only partially [42] or the analysis is preliminary [43,65], but the main results were presented in terms of the steady-state molecular formation rate $\tilde{\lambda}_{dd\mu}$, i.e., the rate after dynamical equilibrium between the two $d\mu$ hyperfine states has been reached. In pure D_2 the steady-state $d\mu(F)$ populations P_F ($\sum_F P_F = 1$) are given by [36]

$$\frac{P_{3/2}}{P_{1/2}} = \frac{(\tilde{\lambda}_{1/2,3/2} + \frac{2}{3}\tilde{\lambda}_{1/2})}{(\tilde{\lambda}_{3/2,1/2} + \frac{1}{3}\tilde{\lambda}_{3/2})} \tag{30}$$

and

$$\tilde{\lambda}_{dd\mu} = \sum_F P_F \tilde{\lambda}_F \ . \tag{31}$$

The rates given in Ref. [38] were derived from a measurement in deuterium-tritium (DT) mixtures, where the steady-state populations P_F depend on the complete kinetics of the much more complicated μCF in DT and correspond to a not-so-well-defined average between $\tilde{\lambda}_{1/2}$ and $\tilde{\lambda}_{3/2}$. However, at temperatures $\gtrsim$ 400 K $\tilde{\lambda}_{1/2}$ and $\tilde{\lambda}_{3/2}$ coincide within the experimental error and can both be equated to $\tilde{\lambda}_{dd\mu}$.

In order to compare all data on an equal footing, $\tilde{\lambda}_{dd\mu}$ for the Vienna-PSI data was calculated according to Eqs. (30) and (31). The inverse hyperfine rate $\tilde{\lambda}_{1/2,3/2}$ was determined by the detailed-balance relation equation (18). The solid line in Fig. 8 is $\tilde{\lambda}_{dd\mu}$ computed from the fits to $\tilde{\lambda}_F$ and $\tilde{\lambda}_{3/2,1/2}$, where for the latter we used the parameters in Table VII, fit (a). Note that in spite of the fact that the extrapolation of $\tilde{\lambda}_{3/2,1/2}$ beyond 150 K is ambiguous, the extrapolation of $\tilde{\lambda}_{dd\mu}$ is well defined because $\tilde{\lambda}_{dd\mu}$ depends only weakly on $\tilde{\lambda}_{3/2,1/2}$: the changes in $\tilde{\lambda}_{dd\mu}$, when using the theoretical instead of the fitted $\tilde{\lambda}_{3/2,1/2}$, never exceed 1.5%.

By and large, fair agreement of the other experiments with the results for our analysis is found, although some significant discrepancies remain at low temperatures. In the range 20 K $< T <$ 60 K, which is dominated by nonresonant molecular formation, experiment [43] agrees with the Vienna-PSI data, while the point from Ref. [42] lies by a factor of 2 above both other experiments and also strongly disagrees with theory. At the beginning of the sharp rise of $\tilde{\lambda}_{dd\mu}$ in the range 60–90 K, three points lie significantly above our fit. At higher temperatures discrepancies reduce to between 1 and 3σ. Quite remarkably, agreement of the extrapolation from the Vienna-PSI data with several accurate measurements at room temperature is within 1σ (inset in Fig. 8) and even the extrapolation up to 600 K agrees with experiment [38] within 3σ at worst. This agreement far beyond the fit range $\leq$ 150 K further supports the general theoretical description of $dd\mu$ molecular formation. In particular, major errors in the size of the formation matrix elements for low temperatures relative to those for higher temperatures, which would distort the extrapolation, can be excluded.

In view of the agreement at higher temperatures it will be very interesting to investigate origin and implications of the discrepancies between some of the low-temperature data once an analysis of all data in terms of the rates $\tilde{\lambda}_F$ and $\tilde{\lambda}_{3/2,1/2}$ and of the physical parameters λ_{nr}, ε_{11}, and $\tilde{\lambda}_f$ will be available.

VI. CONCLUSIONS

The careful analysis of the Vienna-PSI experiment [41] shows that by now the basic theoretical picture of μCF in pure deuterium is nearly complete.

The recent calculation of the nonresonant formation rate is compatible with our experimental findings. Theoretical resonant molecular formation rates agree with the Vienna-PSI low-temperature data after minor adjustments of the molecular formation matrix elements, or, alternatively, of the effective fusion rate. The theoretical description of $dd\mu$ formation is confirmed by the agreement of the theory-based extrapolation from $T \leq 150$ K with data up to 600 K, although discrepancies between experiments at temperatures 50–90 K still await clarification.

The most significant result of our analysis is the accurate extraction of the $dd\mu$ binding energy ε_{11} largely independent of other parameters. The experimental and theoretical values of ε_{11} coincide well within the limits of ± 0.5 meV, which are set by our knowledge of the nuclear-structure parameters of the deuteron. The agreement amounts to a few percent of vacuum polarization in $dd\mu$ and is still within fractions of various kinds of relativistic and nuclear-structure corrections.

The most significant discrepancy between theory and

experiment is found for the hyperfine rates. This is particularly deplorable since combining experimental results for the back-decay contribution to the hyperfine rates $\lambda^{\rm back}_{3/2,1/2}$ with the effective molecular formation rates $\tilde{\lambda}_F$ would allow one to determine the effective *dd* fusion rate $\tilde{\lambda}_f$ and the $dd\mu$ formation matrix elements $|V_{if}|$. Since the contribution of $dd\mu$ deexcitation to $\tilde{\lambda}_f$ is small and the factor from the $dd\mu$ wave function which enters the fusion rate is well known, an experimental value for $\tilde{\lambda}_f$ would supply unique information about the *dd* fusion reaction at very low energies. This would supplement and test the present models of this reaction, which are based on a vast amount of data at higher energies [66]. On the other hand, the delicate problems involved in the theoretical description of $[(dd\mu)dee]$ formation through a low-energy rearrangement reaction, which were addressed in Refs. [36,59], call for an independent experimental determination of the formation matrix elements $|V_{if}|$.

Therefore a clear identification of the back-decay contribution $\lambda^{\rm back}_{3/2,1/2}$ to the experimental rates $\tilde{\lambda}_{3/2,1/2}$ is highly desirable. Obviously, a theoretical reexamination of low-energy $d\mu+D_2$ spin-flip scattering should be undertaken. In experiments, the reduction of the statistical errors and measurements over a larger temperature range would allow one to more clearly separate $\lambda^{\rm back}_{3/2,1/2}$ and $\lambda^{\rm scat}_{3/2,1/2}$ on the grounds of their different temperature dependence. While in such a separation the shape of $\lambda^{\rm back}_{3/2,1/2}$ is determined by the observed formation rate, the shape of $\lambda^{\rm scat}_{3/2,1/2}$ has to be drawn from theory, which is quite unsatisfactory in view of the existing discrepancy.

A purely experimental discrimination between $\lambda^{\rm back}_{3/2,1/2}$ and $\lambda^{\rm scat}_{3/2,1/2}$ will be attempted in an experiment where in mixtures of protium and deuterium the molecular concentrations of H_2, HD, and D_2 will be varied [67]. The two contributions can be distinguished by using the fact that the resonant $\lambda^{\rm back}_{3/2,1/2}$ depends on the concentration of D_2 molecules, while the charge exchange rate $\lambda^{\rm scat}_{3/2,1/2}$ is proportional to the concentration of deuterons irrespective of their molecular binding.

An independent determination of $\lambda^{\rm back}_{3/2,1/2}$ would also allow one to decide whether $\lambda^{\rm back}_{3/2,1/2}$ can be responsible for the nontrivial density dependence of $\tilde{\lambda}_{3/2,1/2}$ observed at the transition from gas to liquid. In that case a comparable density effect should exist in $\tilde{\lambda}_{3/2}$, which has not been found, but at present —due to the experimental errors of $\tilde{\lambda}_{3/2}$– cannot be ruled out either.

By and large, for molecular formation rates, theory and experiments have reached a comparable level of accuracy and agree satisfactorily. At least three interesting physical problems –low-energy *dd* fusion, the low-energy $[(dd\mu)dee]$ formation reaction, and resonance broadening and density effects in $dd\mu$ formation—strongly motivate further attempts to resolve the discrepancy between theoretical and experimental hyperfine transition rates.

ACKNOWLEDGMENTS

Support by the Austrian Science Foundation and the Paul Scherrer Institute is gratefully acknowledged. We want to thank Dr. C. Petitjean for a long and fruitful collaboration in the experiments on which the present theoretical analysis is based. We are grateful to Dr. A. Adamczak, Dr. D. D. Bakalov, Dr. L. N. Bogdanova, Dr. V. E. Markushin, Dr. V. S. Melezhik, and Dr. L. I. Men'shikov for numerous valuable discussions. Finally, it is our pleasure to express our gratitude to Professor J. P. Blaser and Professor K. Lintner for many years of support and encouragement.

APPENDIX A: FUSION AND BACK-DECAY FRACTIONS

The numbers of fusions and back decays up to time t after $[(dd\mu)dee]\equiv$MD formation, denoted by $n_f(t)$ and $n_F(t)$, respectively, evolve in time according to

$$\frac{dn_f(t)}{dt}=\sum_K n_K(t)\tilde{\lambda}_f \ , \tag{A1}$$

$$\frac{dn_F(t)}{dt}=\sum_K n_K(t)\Gamma_{SK,F} \ , \tag{A2}$$

where n_K are the populations of the individual rotational states $(\mathrm{MD})_K$ and the total back-decay rate from a given rotational state K is defined by $\Gamma_{SK,F}\equiv\sum_{K_i}\Gamma_{SK,FK_i}$. The total yields are obtained by integration,

$$\begin{aligned} n_f(\infty)-n_f(0)&=\sum_K I_K\tilde{\lambda}_f \ , \\ n_F(\infty)-n_F(0)&=\sum_K I_K\Gamma_{SK,F} \ , \end{aligned} \tag{A3}$$

where we defined the integrals $I_K:=\int_0^\infty n_K(t)dt$.

The populations $n_K(t)$ evolve according to the linear differential equations

$$\frac{dn_K}{dt}=-\left[\tilde{\lambda}_f+\sum_F\Gamma_{SK,F}+\Lambda_K\right]n_K + \sum_{K'\neq K}\Lambda_{K'K}n_{K'} \ , \tag{A4}$$

where the total loss rate from a given rotational state is composed of fusion ($\tilde{\lambda}_f$), back decay to both hyperfine states ($\sum_F\Gamma_{SK,F}$), and the total rotational transition rate Λ_K; the state K in turn is fed by transitions from the other rotational states K' with rates $\Lambda_{K'K}$. (Clearly, $\Lambda_K=\sum_{K'}\Lambda_{KK'}$.)

Integrating Eq. (A4) yields

$$n_K(\infty)-n_K(0)=\sum_{K'}\mathcal{T}_{KK'}I_{K'} \ , \tag{A5}$$

where we defined the time evolution matrix

$$\mathcal{T}_{KK'}:=-\left[\tilde{\lambda}_f+\sum_F\Gamma_{SK,F}+\Lambda_K\right]\delta_{KK'}+\Lambda_{K'K} \ . \tag{A6}$$

We observe that $n_K(\infty)=0$, since eventually all MD states will decay. The integrals $I_K(K_f)$ with the initial condition $n_K(0)=\delta_{KK_f}$ are now obtained from Eq. (A5) as

$$I_K(K_f)=-(\mathcal{T}^{-1})_{KK_f} \ . \tag{A7}$$

By substituting (A7) into (A3) we see that, if we initially populate a state $(MD)_{K_f}$, a fraction of

$$w_S^{\rm fus}(K_f) = -\sum_K (\mathcal{T}^{-1})_{KK_f}\tilde{\lambda}_f \tag{A8}$$

will fuse, while the fractions

$$w_{SF'}^{\rm back}(K_f) = -\sum_K (\mathcal{T}^{-1})_{KK_f}\Gamma_{SK,F'} \tag{A9}$$

will decay back to $d\mu(F')+D_2$.

Equation (12) for $\tilde{\lambda}_f$, $\Gamma_{SK,F} \gg \lambda_{KK'}$ trivially follows, if we set $\Lambda_{KK'} \equiv 0$. In the other limit $\Lambda_{KK'} \to \infty$ the right-hand side of (A4) diverges unless

$$-\Lambda_K n_K + \sum_{K'} \Lambda_{K'K} n_{K'} = 0 \ . \tag{A10}$$

This is just the condition of thermal equilibrium between the populations. By substituting Boltzmann populations $n_K(t) = \omega_f(K) n(t)$ and summing over K, Eq. (A4) can be readily solved for $n(t)$ and from Eq. (A3) one obtains Eq. (13).

In the derivation above we did not distinguish between the individual z components of K_f. Yet at very low densities, when transitions between K_f states are slow, also transitions between individual K_{fz} states must be expected to be suppressed so that in the molecular complex K_f and J increasingly tend to remain coupled together to the total angular momentum $\mathcal{J} = \mathbf{K}_f + \mathbf{J}$ (as pointed out in [55]). As a result our expressions for $w^{\rm fus}$ and $w^{\rm back}$ in Eqs. (A8) and (A9) are only approximations which will become inaccurate at low target densities. A quantitative assessment of the effect was not possible at present since no detailed theoretical, let alone experimental values for collision-induced transition rates between magnetic states of the excited complex MD are available (cf. Ref. [60]). Thus, further studies are necessary to accurately describe resonant $dd\mu$ formation at very low densities.

APPENDIX B: DETAILED BALANCE FOR $\lambda_{FF'}$

In the limiting case $\tilde{\lambda}_f$, $\Gamma_{SK,F} \ll \Lambda_{KK'}$ we obtain the fusion fraction equation (13) and, analogously, the back-decay fraction

$$w_{SF'}^{\rm back}(K_f) \approx \Gamma_{SF'} \Big/ \left[\tilde{\lambda}_f + \sum_{F''} \lambda_{SF''} \right] , \tag{B1}$$

where Γ_{SF} is defined by

$$\Gamma_{SF} \equiv \sum_{K_i K_f} \omega_f(K_f) \Gamma_{SK_f,FK_i} \tag{B2}$$

with the Boltzmann distribution of the rotational states of the MD molecule

$$\begin{aligned} \omega_f(K_f) &= [(2K_f+1)\exp(-E_{\rm MD}(K_f)/k_BT)]/Z_f \ , \\ Z_f &= \sum_{K_f} (2K_f+1)\exp[-E_{\rm MD}(K_f)/k_BT] . \end{aligned} \tag{B3}$$

In that case we can sum over K_i and K_f in Eq. (17) to obtain

$$\lambda_{FF'}^{\rm back} = \sum_S \frac{\lambda_{FS}\Gamma_{SF'}}{\tilde{\lambda}_f + \sum_{F''} \Gamma_{SF''}} \tag{B4}$$

with $\lambda_{FS} := \sum_{K_i K_f} \lambda_{FK_i,SK_f}$.

If the D_2 rotational states are in thermal equilibrium we have

$$\begin{aligned} \omega_i(K_i) &= [(2K_i+1)\xi(K_i)\exp(-E_{D_2}(K_i)/k_BT)]/Z_i \ , \\ Z_i &= \sum_{K_i} (2K_i+1)\xi(K_i)\exp[-E_{D_2}(K_i)/k_BT] \ . \end{aligned} \tag{B5}$$

By expressing ε_{if} in Eq. (3) through Eq. (2) and using Eq. (10) one gets the relation between formation and back-decay rates

$$\lambda_{FK_i,SK_f} = N \left[\frac{2\pi}{mk_BT} \right]^{3/2} \frac{2S+1}{2F+1} \frac{2K_f+1}{Z_i} \exp\left[-\frac{\varepsilon_{11} + \delta\varepsilon_{dd\mu}(S) + E_{\rm MD}(K_f) - \delta\varepsilon_{d\mu}(F)}{k_BT} \right] \Gamma_{SK_f,FK_i} \ . \tag{B6}$$

Using Eqs. (B2) and (B5) we perform the sum over the K_i and K_f to obtain the following relation between λ_{FS} and Γ_{SF}:

$$\lambda_{FS} = N \left[\frac{2\pi}{mk_BT} \right]^{3/2} \frac{2S+1}{2F+1} \frac{Z_f}{Z_i} \exp\left[-\frac{\varepsilon_{11} + \delta\varepsilon_{dd\mu}(S) - \delta\varepsilon_{d\mu}(F)}{k_BT} \right] \Gamma_{SF} \ . \tag{B7}$$

After inserting (B7) into (B4) one obtains

$$\lambda_{FF'}^{\rm back} / \lambda_{F'F}^{\rm back} = \frac{2F'+1}{2F+1} \exp\left[-\frac{\delta\varepsilon_{d\mu}(F') - \delta\varepsilon_{d\mu}(F)}{k_BT} \right] , \tag{B8}$$

which is the detailed-balance ratio. Since it is known that the same relation holds for $\lambda_{FF'}^{\rm scat}$ it follows that Eq. (18) becomes exact for $\tilde{\lambda}_f$, $\Gamma_{SK,F} \ll \Lambda_{KK'}$.

[1] W. H. Breunlich, P. Kammel, J. S. Cohen, and M. Leon, Annu. Rev. Nucl. Part. Sci. **39**, 311 (1989).

[2] L. I. Ponomarev, Contemp. Phys. **31**, 219 (1991).

[3] V. P. Dzhelepov *et al.*, Zh. Eksp. Teor. Fiz. **50**, 1235 (1966) [Sov. Phys. JETP **23**, 820 (1966)].

[4] E. A. Vesman. Pis'ma Zh. Eksp. Teor. Fiz. **5**, 113 (1967) [JETP Lett. **5**, 91 (1967)].

[5] S. I. Vinitsky and L. I. Ponomarev, Fiz. Elem. Chastits At.

Yadra **13**, 1336 (1982) [Sov. J. Part. Nucl. **13**, 557 (1982)].
[6] L. I. Ponomarev, I. V. Puzynin, and T. P. Puzynina, Zh. Eksp. Teor. Fiz. **65**, 28 (1973) [Sov. Phys. JETP **38**, 14 (1973)].
[7] S. I. Vinitsky *et al.*, Zh. Eksp. Teor. Fiz. **79**, 698 (1980) [Sov. Phys. JETP **52**, 353 (1980)].
[8] A. D. Gocheva *et al.*, Phys. Lett. **153B**, 349 (1985).
[9] S. I. Vinitsky *et al.*, Zh. Eksp. Teor. Fiz. **74**, 849 (1978) [Sov. Phys. JETP **47**, 444 (1978)].
[10] V. M. Bystritsky *et al.*, Zh. Eksp. Teor. Fiz. **76**, 460 (1979) [Sov. Phys. JETP **49**, 232 (1979)].
[11] P. Kammel *et al.*, Phys. Lett. **112B**, 319 (1982); Phys. Rev. A **28**, 2611 (1983).
[12] D. D. Bakalov, Zh. Eksp. Teor. Fiz. **79**, 1149 (1980) [Sov. Phys. JETP **52**, 581 (1980)]; D. D. Bakalov *et al.*, *ibid.* **79**, 1629 (1980) [*ibid.* **52**, 820 (1980)].
[13] V. S. Melezhik, Pis'ma Zh. Eksp. Teor. Fiz. **36**, 101 (1982) [JETP Lett. **36**, 125 (1982)].
[14] M. P. Leon, Phys. Rev. Lett. **52**, 605 (1984).
[15] M. P. Faifman *et al.*, Z. Phys. D **2**, 79 (1986).
[16] A. Scrinzi, K. Szalewicz, and H. J. Monkhorst, Phys. Rev. A **37**, 2270 (1988).
[17] J. Cohen and R. L. Martin, Phys. Rev. Lett. **53**, 738 (1984).
[18] M. P. Leon and J. S. Cohen, Phys. Rev. A **31**, 2680 (1985).
[19] D. D. Bakalov *et al.*, Zh. Eksp. Teor. Fiz. **94**, 61 (1988) [Sov. Phys. JETP **67**, 1990 (1988)].
[20] L. N. Bogdanova *et al.*, Phys. Lett. **115B**, 171 (1982); **167B**, 485E (1986).
[21] V. N. Ostrovskii and V. I. Ustimov, Zh. Eksp. Teor. Fiz. **79**, 1228 (1980) [Sov. Phys. JETP **52**, 620 (1980)].
[22] A. M. Lane, Phys. Lett. **98A**, 337 (1983).
[23] A. Gula, A. Adamczak, and M. Bubak, Phys. Lett. **109A**, 224 (1985).
[24] M. Leon, Phys. Rev. A **33**, 4434 (1986).
[25] V. S. Melezhik and J. Wozniak, Phys. Lett. **116A**, 370 (1986); L. Bracci *et al.*, Muon Catalyzed Fusion **4**, 247 (1989).
[26] A. M. Frolov and V. D. Efros, Yad. Fiz. **41**, 828 (1985) [Sov. J. Nucl. Phys. **41**, 528 (1985)].
[27] S. I. Vinitsky *et al.*, Zh. Eksp. Teor. Fiz. **91**, 705 (1986) [Sov. Phys. JETP **64**, 417 (1986)].
[28] K. Szalewicz *et al.*, Phys. Rev. A **36**, 5494 (1987).
[29] M. Kamimura, Phys. Rev. A **38**, 621 (1988).
[30] S. A. Alexander and H. J. Monkhorst, Phys. Rev. A **38**, 26 (1988); **39**, 3705E (1989).
[31] D. D. Bakalov *et al.*, Phys. Lett. **161B**, 5 (1985); Muon Catalyzed Fusion **3**, 321 (1988).
[32] D. Bakalov and V. I. Korobov, J. Inst. Nucl. Res. Rapid Comm. **2**, 15 (1989).
[33] K. Swe Myint *et al.*, Z. Phys. A **334**, 423 (1989).
[34] G. Aissing, D. D. Bakalov, and H. J. Monkhorst, Phys. Rev. A **42**, 116 (1990).
[35] L. I. Men'shikov and M. P. Faifman, Yad. Fiz. **43**, 650 (1986) [Sov. J. Nucl. Phys. **43**, 414 (1986)].
[36] L. I. Men'shikov *et al.*, Zh. Eksp. Teor. Fiz. **92**, 1173 (1987) [Sov. Phys. JETP **65**, 656 (1987)].
[37] D. V. Balin *et al.*, Phys. Lett. **141B**, 173 (1984); Pis'ma Zh. Eksp. Teor. Fiz. **40**, 318 (1984) [JETP Lett. **40**, 112 (1984)].
[38] S. E. Jones *et al.*, Phys. Rev. Lett. **56**, 588 (1986).
[39] M. Cargnelli, Ph.D. thesis, Technical University of Vienna, Vienna, 1986 (unpublished); M. Cargnelli *et al.*, in *Proceedings of the Twenty-Third Yamada Conference on Nuclear Weak Processes and Nuclear Structure, Osaka, 1989,* edited by M. Morita, E. Ejiri, H. Ohtsubo, and T. Sato (World Scientific, Singapore, 1989), p. 115.
[40] N. Nägele *et al.*, Nucl. Phys. **439A**, 397 (1989).
[41] J. Zmeskal *et al.*, Muon Catalyzed Fusion **1**, 109 (1987); Phys. Rev. A **42**, 1165 (1990).
[42] D. V. Balin *et al.*, Muon Catalyzed Fusion **5**, 163 (1990).
[43] V. M. Bystritsky *et al.*, Muon Catalyzed Fusion **5**, 141 (1990).
[44] M. P. Faifman *et al.*, Muon Catalyzed Fusion **4**, 1 (1989).
[45] L. I. Menshikov, Yad. Fiz. **42**, 1449 (1985) [Sov. J. Nucl. Phys. **42**, 918 (1985)].
[46] D. D. Bakalov, Muon Catalyzed Fusion **3**, 321 (1988).
[47] A. Scrinzi and K. Szalewicz, Phys. Rev. A **39**, 4983 (1989).
[48] P. C. Souers, *Hydrogen Properties for Fusion Energy* (California Univ. Press, Berkeley, 1985), p. 308.
[49] Yu. V. Petrov. Phys. Lett. **163B**, 28 (1985); V. Yu. Petrov and Yu. V. Petrov, Muon Catalyzed Fusion **4**, 73 (1989).
[50] L. I. Men'shikov, Fiz. Elem. Chastits At. Yadra **19**, 1349 (1988) [Sov. J. Part. Nucl. **19**, 583 (1988)].
[51] M. P. Faifman, L. I. Men'shikov, and L. I. Ponomarev, Muon Catalyzed Fusion **2**, 247 (1988).
[52] J. S. Cohen and M. Leon, Phys. Rev. A **39**, 946 (1989); M. Leon, *ibid.* **39**, 5554 (1989).
[53] L. I. Ponomarev and M. P. Faifman, Zh. Eksp. Teor. Fiz. **71**, 1689 (1976) [Sov. Phys. JETP **44**, 886 (1976)].
[54] M. P. Faifman, Muon Catalyzed Fusion **4**, 341 (1989).
[55] M. Leon, Muon Catalyzed Fusion **5**, 127 (1990); and private communication.
[56] N. T. Padial, J. S. Cohen, and R. B. Walker, Phys. Rev. A **37**, 329 (1988).
[57] A. M. Lane, in *Muon-Catalyzed Fusion and Fusion with Polarized Nuclei,* Proceedings of the Eighth Course of the International School of Fusion Reactor Technology "Ettore Majorana," Erice, 1987, edited by B. Brunelli and G. G. Leotta (Plenum, New York, 1987), Vol. 33, p. 67.
[58] J. Lukasik and J. Ducuing, J. Chem. Phys. **60**, 331 (1974).
[59] A. Scrinzi, Ph.D. dissertation, University of Vienna, Vienna, 1989 (unpublished); A. Scrinzi, Muon Catalyzed Fusion **5**, 179 (1990).
[60] N. T. Padial, J. Cohen, and M. Leon, Phys. Rev. A **38**, 1172 (1988); M. P. Auzin'sh and R. S. Ferber, Usp. Fiz. Nauk **160**, 73 (1990) [Sov. Phys. Usp. **33**, 833 (1990)].
[61] A. Adamczak, Muon Catalyzed Fusion **5**, 65 (1990).
[62] J. Cohen, Phys. Rev. A **43**, 4668 (1991).
[63] L. Bracci, G. Fiorentini, and R. Trippicione, Nucl. Phys. **217B**, 215 (1983).
[64] L. Bogdanova (private communication).
[65] V. V. Filchenkov and L. Marczis, Muon Catalyzed Fusion **6**, 499 (1991).
[66] G. Hale, Muon Catalyzed Fusion **5**, 227 (1990).
[67] Ackerbauer *et al.*, PSI proposal, addendum, No. R-81-05.2, 1990 (unpublished).